Nuclear Engineering and Technology 54 (2022) 226–233

Contents lists available at ScienceDirect

Nuclear Engineering and Technology

journal homepage: www.elsevier.com/locate/net

Original article

Phase-field simulation of radiation-induced bubble evolution in recrystallized U–Mo alloy

Yanbo Jiang [a], Yong Xin [b], Wenbo Liu [a, *], Zhipeng Sun [b], Ping Chen [b, **], Dan Sun [b], Mingyang Zhou [b], Xiao Liu [c], Di Yun [a]

[a] Department of Nuclear Science and Technology, Xi'an Jiaotong University, Xi'an, 710049, China
[b] Science and Technology on Reactor System Design Technology Laboratory, P.O. Box 502, Chengdu, 610213, China
[c] Institute of Nuclear Physics and Chemistry, China Academy of Engineering Physics, Jiangyou, 621907, China

ARTICLE INFO

Article history:
Received 25 January 2021
Received in revised form
16 July 2021
Accepted 19 July 2021
Available online 20 July 2021

Keywords:
Phase-field
U–Mo
Bubble
Recrystallization
Fission density

ABSTRACT

In the present work, a phase-field model was developed to investigate the influence of recrystallization on bubble evolution during irradiation. Considering the interaction between bubbles and grain boundary (GB), a set of modified Cahn-Hilliard and Allen-Cahn equations, with field variables and order parameters evolving in space and time, was used in this model. Both the kinetics of recrystallization characterized in experiments and point defects generated during cascade were incorporated in the model. The bubble evolution in recrystallized polycrystalline of U–Mo alloy was also investigated. The simulation results showed that GB with a large area fraction generated by recrystallization accelerates the formation and growth of bubbles. With the formation of new grains, gas atoms are swept and collected by GBs. The simulation results of bubble size and distribution are consistent with the experimental results.

1. Introduction

The development of new high-density fuels with low-enriched uranium, which can be used in research reactors, has been extensively investigated to preventing nuclear proliferation in the past decades [1,2]. U–Mo alloys are currently being developed as a potential candidate fuel due to their good phase stability, good radiation resistance, simple post-processing and high uranium density that can reach 8–9 g/cm^3 [3,4]. However, at high fission density, the fuel and cladding are likely to interact mechanically due to fuel swelling. It is accepted that the formation of gas bubbles is the main reason of fuel swelling. Therefore, it is crucial to understand and analyze the mechanism of the behavior of fission gas bubbles under irradiation.

Gaseous species, such as Xe and Kr generated by fission reactions of uranium, tend to accumulate in voids to form gas bubbles due to their low solubilities in metal fuels [5]. On the one hand, the production of point defect, such as vacancy, interstitial and gas atom by collision cascades, determines the formation and growth of bubbles. On the other hand, existing microstructural features of materials, including grain boundaries (GBs), dislocation networks and precipitates, significantly affect the evolution of bubbles. These two common factors control the processes of nucleation, growth, migration and coalescence of gas bubbles in U–Mo alloy. However, a thorough understanding of the interaction between point defects and microstructural features is still an essential subject in the field of nuclear reactor fuel materials, since they are closely related to gas behaviors.

What cannot be ignored is that, at a fission density of approximately 3.0 × 10^{21} f/cm^{-3}, a fission-induced phenomenon called grain subdivision or recrystallization occurs spontaneously in nuclear fuels [6,7]. During recrystallization, large fuel grains with a size of several microns are subdivided into small grains, and intragranular bubbles will highly likely collapse and coalesce into intergranular bubbles, leading to extreme swelling in U–Mo alloy. These recrystallized grain structures lead to the increase of area fraction of GB and decrease of the gas atom diffusion distance from GB to the grain interior, which drastically accelerates the formation and growth of bubbles. Although the detailed mechanisms causing recrystallization are still under debate, it was commonly accepted that the recrystallization mainly starts on GB or free surfaces and

* Corresponding author.
** Corresponding author.
E-mail addresses: liuwenbo@xjtu.edu.cn (W. Liu), chenping_npic@163.com (P. Chen).

https://doi.org/10.1016/j.net.2021.07.034

then moves to the center of the grain and fills the whole grain eventually [8–12]. As a result, the initial grain with high dislocation density tend to refine [11,13] and there is a reason to believe that the driving force of recrystallization is the minimization of the local energy of the system [14–16].

As a supplement and guidance to experiments, computer simulation methods play a pivotal role in the field of nuclear fuels research. A number of molecular dynamics (MD) simulations were used to investigate the thermodynamic and kinetic properties of gas bubble in U–Mo [17,18]. Rate theory, as a dynamic method, has been applied in the investigations of recrystallization in U–Mo alloy [19,20], but in-depth analyses of thermodynamics was not conducted. In the mesoscopic scale, phase-field method is advantageous as its drive force is the reduction of free energy in the system, and it has been applied successfully in the investigations of fuel performance [21], grain growth [22,23], void and gas bubble evolution [24–26] and recrystallization [27–30] during irradiation. Considering the strain energy at deformed grains, Abdoelatef et al. [27] developed a phase-field model to simulate the formation and evolution of high burn-up structure. Their results demonstrated that the density and distribution of dislocation, GB energy and existing bubbles strongly affect recrystallization. However, the bubbles were directly introduced in their model, and the evolution of bubble was ignored. Liang et al. [29] developed a phase-field model to simulate the evolution of intergranular gas bubbles and the recrystallization process. Their results showed that the recrystallization process increases the nucleation rate of gas bubbles. However, it was still a scant of phase-field simulation to investigate the micromorphology of the gas bubble evolution and distribution with the influence of recrystallization at different fission densities.

In the present work, a phase-field model was developed which contains a couple of conserved phase-field variables c_v, c_g and a set of non-conserved order parameters η, ϕ_i^d, ϕ_i^r. The formulation of free energy was modified to incorporate the interaction between bubbles and GB. The kinetics of recrystallization from experimental data was also considered. This simulation of microstructural evolution under irradiation is governed by a set of modified Cahn-Hilliard and Allen-Cahn equations. Firstly, the growth of a single bubble with supersaturated point defect concentration was analyzed with the corresponding equilibrium concentration of gas atoms. In addition, the phase-field model was applied in polycrystalline to investigate the bubble evolution in recrystallized U–Mo alloy. The size and distribution of bubbles obtained from the simulation result were consistent with the experimental observation.

2. Phase-field model

Considering the evolution of gas bubbles and recrystallized grain growth, a mesoscale phase-field model is presented in this section. A couple of conserved field variables were considered in the phase-field model to simulate the bubble evolution in polycrystalline U–Mo alloy: a vacancy concentration $c_v(r,t)$ and a gas atom concentration $c_g(r,t)$. The vacancies and Xe gas atoms introduced by cascade collision, which can diffuse and grow into gas bubbles, are considered in these two variables. Two stable phases, namely a bubble phase with $c_v = 1.0$, $c_g \neq 0.0$ and an initial microstructure of matrix phase with thermodynamic equilibrium concentration of point defects with $c_v = c_v^{eq}$, $c_g = c_g^{eq}$, are involved in the present work. The temporal and spatial evolution of field variables was driven by diffusion fluxes provided by their corresponding chemical potential gradients. A non-conserved order parameter $\eta(r,t)$ was used to distinguish these two phases in space which takes a value of $\eta = 1.0$ in the bubble phase while $\eta = 0.0$ in the matrix phase. In addition, a set of order parameters ϕ_i^d and ϕ_i^r was used to represent the set of grain orientations of deformed grains and recrystallized grains. The values of the order parameter ϕ_i^d and ϕ_i^r equal to one within a grain while equal to zero within the other grains, similar to Chen's work [31]. All the conserved and non-conserved variables vary smoothly across the respective interface.

In the present phase-field model, a reasonable free energy function of bubble evolution was built based on Xiao's work [32]. In addition, the free energy of deformed grains and recrystallized grains and their interaction with bubbles was considered, too. Following the form of free energy in a non-uniform condition [33], the total free energy of the system with the field variables and order parameters is described by:

$$F = N\int_V \left[f_{bulk}(c_v, c_g, \eta) + f_{poly}\left(\eta, \phi_i^d, \phi_i^r\right) + f_{grad} + f_{stored}\left(\phi_i^d\right)\right] dV \tag{1}$$

where N is the number of lattice sites per unit volume, f_{bulk} is the bulk free energy density describing the difference between bubble phase and matrix phase that depends on the composition and fraction of the point defects, f_{poly} is the polycrystalline energy density and f_{grad} is the gradient energy, respectively. f_{store} is the stored elastic energy density provided by dislocation density that is related to recrystallization.

The bulk free energy density used for the bubble evolution is written as

$$f_{bulk}(c_v, c_g, \eta) = h(\eta) f^m(c_v, c_g) + j(\eta) f^b(c_v, c_g) \tag{2}$$

where $h(\eta)$ and $j(\eta)$ are interpolating functions used to describe the fraction of the bubble phase with the forms $h(\eta) = (\eta - 1)^2$ and $j(\eta) = \eta^2$. It is clear that $h(\eta) = 1.0$ at $\eta = 0.0$ in the matrix phase and $j(\eta) = 1.0$ at $\eta = 1.0$ in the bubble phase which ensures the free energy vary smoothly in the interface between the matrix phase and the bubble phase. The matrix phase free energy based on regular solution model is derived from the enthalpy and entropic formulation of vacancy and gas atom in the matrix that is described in [32].

$$f^m(c_v, c_g) = k_B T\left[c_v \ln\frac{c_v}{c_v^{eq}} + c_g \ln\frac{c_g}{c_g^{eq}} + (1 - c_v - c_g)\ln\frac{1 - c_v - c_g}{1 - c_v^{eq} - c_g^{eq}}\right] \tag{3}$$

where k_B is Boltzmann's constant, c_v^{eq} and c_g^{eq} are the thermodynamic equilibrium concentration of vacancy and Xe gas atom with forms $c_v^{eq} = \exp(-E_v^f/k_BT)$ and $c_g^{eq} = \exp(-E_g^f/k_BT)$ in the matrix phase, respectively, where E_v^f and E_g^f are the vacancy and gas atom formation energy.

Considering the configuration of gas atom in a bubble where $\eta = 1.0$ is assumed, the free energy of bubble phase is written as [32].

$$f^b(c_v, c_g) = k_B T\left[c_v \ln\frac{c_v}{c_v^b} + (1 - c_v)\ln\frac{1 - c_v}{1 - c_v^b} + c_g \ln\frac{c_g}{c_g^b} + \left(c_g^m - c_g\right)\ln\frac{c_g^m - c_g}{c_g^m - c_g^b}\right] \tag{4}$$

where c_v^b and c_g^b are the equilibrium concentrations of vacancy and gas atom in a bubble, c_v^b is set to 0.99 for stability, c_g^b is derived based

on the van der Waals equation of state under high pressure, c_g^m is the maximum gas atom concentration based on the volume of a U–Mo molecule and the van der Waals constant with a form $c_g^m = \Omega/b$, respectively. The formulation of bulk free energy density is strictly based on the thermodynamic theory and the detailed derivation has been introduced in Wang 's work [34].

The deformed grains are represented by a set of order parameters ϕ_i^d, while the recrystallized grains are represented by ϕ_i^r. The polycrystalline free energy is written as [27].

$$f^{poly}\left(\eta,\phi_i^d,\phi_i^r\right) = A\left[\frac{1}{4}\left(\sum_i\left(\phi_i^d\right)^4+\sum_i\left(\phi_i^r\right)^4+\eta^4\right)-\frac{1}{2}\left(\sum_i\left(\phi_i^d\right)^2+\sum_i\left(\phi_i^r\right)^2+\eta^2\right)+\gamma_r\sum_i\sum_{j>i}\left(\phi_i^r\right)^2\left(\phi_j^r\right)^2+\gamma_d\sum_i\sum_{j>i}\left(\phi_i^d\right)^2\left(\phi_j^d\right)^2 + \gamma_{rd}\sum_i\sum_j\left(\phi_i^r\right)^2\left(\phi_j^d\right)^2+\gamma_b\eta^2\left(\sum_i\left(\phi_i^d\right)^2+\sum_i\left(\phi_i^r\right)^2\right)\right] \tag{5}$$

where A is a constant and γ is a set of constants that are defined by the forms $\gamma_r = \gamma_d = \gamma_{ra} = 1.5$ and $\gamma_b = \gamma_r E_{surf}/E_{GB}$ where E_{surf} is the surface energy and E_{GB} is the GB energy [28]. This formulation dictates that the free energy in GB and bubble free surface be higher than that in the grain interior.

The gradient energy term that represents the interfacial free energy of system due to bubble free surfaces and GBs is written as

$$f_{grad}\left(c_v,c_g,\eta,\phi_i^d,\phi_i^r\right) = \frac{\kappa_{c_v}}{2}|\nabla c_v|^2+\frac{\kappa_{c_g}}{2}|\nabla c_g|^2 + \frac{\kappa_\eta}{2}|\nabla\eta|^2+\frac{\kappa_\phi}{2}\left|\nabla\phi_i^d\right|^2+\frac{\kappa_\phi}{2}|\nabla\phi_i^r|^2 \tag{6}$$

where κ_{c_v}, κ_{c_g}, κ_η and κ_ϕ are gradient coefficients for c_v, c_g, η,ϕ_i^d and ϕ_i^r.

The stored elastic energy of dislocation in each damaged grain is written as

$$f_{stored}\left(\phi_i^d\right) = \frac{1}{2}\left(\phi_i^d\right)^2 G b_v^2 \rho_i \tag{7}$$

where G is the shear modulus, b_v is the length of the Burgers vector, and ρ_i is the mean dislocation density in each grain. It should be noted that the dislocation density in recrystallized grain equals zero. In addition, the average dislocation density in grain can be calculated as

$$\rho_i = \frac{1}{V}\int\rho(r,t)h_i(r,t)dV \tag{8}$$

where h_i is the fraction of ith damaged grain with a form described as

$$h_i = \frac{\sum_i\left(\phi_i^d\right)^2}{\sum_i\left(\phi_i^d\right)^2+\sum_j\left(\phi_i^r\right)^2} \tag{9}$$

In the present model, the temporal and spatial evolutions of vacancy and gas atom concentration following the Cahn-Hilliard equation can be written as [35].

$$\frac{\partial c_v}{\partial t} = \nabla\left(M_v\nabla\frac{\delta F}{\delta c_v}\right)+\xi_v+P_v(r,t)-S_v(r,t) \tag{10}$$

$$\frac{\partial c_g}{\partial t} = \nabla\left(M_g\nabla\frac{\delta F}{\delta c_g}\right)+\xi_g+P_g(r,t)-S_g(r,t) \tag{11}$$

where M_v and M_g are the mobility of vacancy and gas atom based on corresponding diffusion coefficient with a form $M_v = \frac{D_v c_v}{k_B T}$ and $M_g = \frac{D_g c_g}{k_B T}$. These couple of modified Cahn-Hilliard formulations are based on the form of the diffusion equation with some additional terms. ξ_v and ξ_g represent the thermal fluctuations of vacancy and gas atom. P_v and P_g are the production of vacancy and gas atom during irradiation, respectively. S_v and S_g represent the absorption of the point defects from dislocations in those deformed grains.

The source term of vacancy P_v which is generated by cascade process is written as [36].

$$P_v(r,t) = \begin{cases} 0 & if \quad \eta \geq 0.8 \ \ or \ \ R_1 > P_{casc} \\ R_2 V_G & if \quad \eta < 0.8 \ \ and \ \ R_1 \leq P_{casc} \end{cases} \tag{12}$$

where P_{casc} is the probability of cascades events at each grid point and time steps which is related to fission density. Respectively, R_1 and R_2 are random numbers with the value of zero to one. V_G is the maximum net increase in vacancy concentration produced by a cascade event and is taken as 0.2 in the present work. In addition, the condition that $\eta < 0.8$ is applied to ensure the source term only works in the matrix phase. The vacancy production rate is defined as

$$K = \overline{V}_G \times P_{casc} \tag{13}$$

where $\overline{V}_G = 0.5V_G$ is the average increase in vacancy concentration. The vacancy production rate K has units of displacements per atom (dpa) per unit time [36]. The damage rate can be connected to the fission rate by a conversion factor B_f with the relation $\dot{f} = B_f K$ [37]. This conversion factor takes a value of $B_f = 2\times10^{23}\ cm^{-3}$ in the present work.

The production of gas atom concentration P_g is written as

$$P_g(r,t) = 2(1-\eta)^2\Lambda\Omega f_r R_3 \tag{14}$$

where Λ is a constant, and Ω is the volume of the lattice site of U–Mo, f_r is the fission rate, R_3 is a random number between zero and one and the number 2 is used to account for the loss of concentration due to the introduction of the random number [25].

S_v and S_g can be written as

$$S_v(r,t) = s_v\left(c_v - c_v^{eq}\right)\Phi \tag{15}$$

$$S_g(r,t) = s_g\left(c_g - c_g^{eq}\right)\Phi \tag{16}$$

where s_v and s_g are a couple of constants that represent the relative absorption strength of the vacancy and gas atom from dislocations, Φ is a formula for dislocation strength in a deformed grain, which is written as

$$\Phi(r,t) = \sum_i \rho_i \left(\phi_i^d\right)^2 \tag{17}$$

where ϕ_i^d equals one in ith deformed grain and ρ_i is the corresponding dislocation density. The order parameters include η that distinguish the bubble from the matrix, and ϕ_i^d, ϕ_i^r that represent different grain orientation are governed by the Allen-Cahn equations [38] as

$$\frac{\partial \eta}{\partial t} = -L\frac{\delta F}{\delta \eta} + \xi_\eta \tag{18}$$

$$\frac{\partial \phi_i^d}{\partial t} = -L\frac{\delta F}{\delta \phi_i^d} \tag{19}$$

$$\frac{\partial \phi_i^r}{\partial t} = -L\frac{\delta F}{\delta \phi_i^r} \tag{20}$$

where ξ_η is a stochastic term. L is the free surface mobility. The values of all parameters are shown in Table .1.

Non-dimensionalized process is essential in numerical implementation. The evolution equations are solved in reduced form with non-dimensional grid spacing ($x = l/l^*$), time step ($\tau = t/t^*$) and diffusivity ($\tilde{D}_v = D_v t^*/l^{*2}$ and $\tilde{D}_g = D_g t^*/l^{*2}$), where the reference system is $l^* = 0.1\mu m$ and $t^* = 10^3 s$. After normalization, the evolution equations are written as

$$\frac{\partial c_v}{\partial \tau} = \tilde{\nabla}\left(\tilde{M}_v \tilde{\nabla}\frac{\delta F}{\delta c_v}\right) + \tilde{\xi}_v + \tilde{P}_v(x,\tau) - \tilde{S}_v(x,\tau) \tag{21}$$

Table 1
Parameters of U–Mo alloy used in the simulation.

Parameter	Symbol	Value	reference
Temperature	T	473K	
Boltzmann's constant	k_B	1.381×10^{-23} J/K	
Grid spacing	x	0.5	This work
Time step	τ	0.001	This work
Lattice constant	a	0.342 nm	[25]
Vacancy diffusion coefficient	D_v	$3.84 \times 10^{-17} m^2/s$	[25]
Gas atom diffusion coefficient	D_g	$4.10 \times 10^{-17} m^2/s$	[39]
Surface mobility	L	9.04×10^{-8} m^3/Js	[25]
Constant	Λ	0.25	[40]
Gradient coefficient	κ_{c_v,c_g}	3.75×10^{-9} J/m	[28]
Gradient coefficient	$\kappa_{\eta,\phi}$	1.36×10^{-8} J/m	[28]
Surface energy	E_{surf}	1.64 Ev	[41]
GB energy	E_{gb}	0.50 Ev	[41]
Xe van der Waals constants	B	0.0516 L/mol	[42]
Shear modulus	G	36.0 GP	[29,43]
Burgers vector	b_v	0.342 nm	[29,44]
Vacancy concentration increase	V_G	0.2	This work

$$\frac{\partial c_g}{\partial \tau} = \tilde{\nabla}\left(\tilde{M}_g \tilde{\nabla}\frac{\delta F}{\delta c_g}\right) + \tilde{\xi}_g + \tilde{P}_g(x,\tau) - S_g(x,\tau) \tag{22}$$

$$\frac{\partial \eta}{\partial \tau} = -\tilde{L}\frac{\delta F}{\delta \eta} + \tilde{\xi}_\eta + \tilde{P}_{v,g}(x,\tau) \tag{23}$$

$$\frac{\partial \phi_i^d}{\partial \tau} = -\tilde{L}\frac{\delta F}{\delta \phi_i^d} \tag{24}$$

$$\frac{\partial \phi_i^r}{\partial \tau} = -\tilde{L}\frac{\delta F}{\delta \phi_i^r} \tag{25}$$

where $\tilde{\nabla} = l^*\nabla$ is the dimensionless gradient operator. In the present study, (15)–(18) are discretized in space with a uniform grid and are solved by using an explicit finite difference method with forward Euler time-stepping. All the stochastic terms are taken as tiny noise.

3. Results and discussion

3.1. Single bubble growth

The growth of a gas bubble is governed by the flux rate of vacancies and gas atoms. In the present model, the driving force of point defects diffusion to a bubble is the chemical potential gradient. An existing bubble keeps its size when the defect concentration in the matrix is the thermodynamic equilibrium concentration. In this situation, the chemical potential in the matrix is equal to that in the bubble $\mu^m = \mu^b$, and the variation of gas atom equilibrium concentration with bubble radius is shown in Fig. 1. This equilibrium concentration is derived from the van der Waals equation under high pressure which is written as [34].

$$c_g^b = \frac{\Omega}{rk_BT/2E_{surf} + b} \tag{26}$$

where r is the bubble radius and b is the van der Waals constant. However, during irradiation, vacancy and gas atom are usually supersaturated. Due to the absorption of vacancies and gas atoms

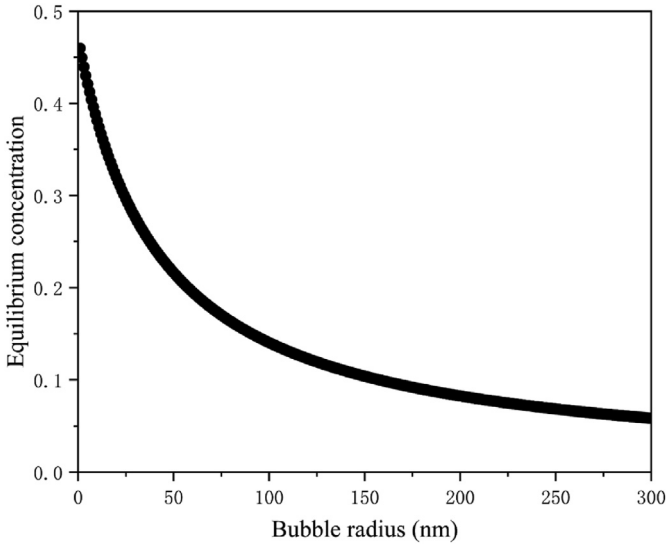

Fig. 1. The gas atom equilibrium concentration changes over bubble radius.

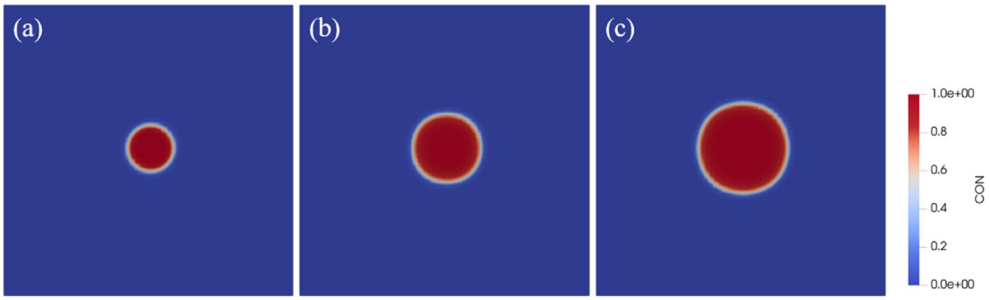

Fig. 2. Single bubble evolution with supersaturated point defects for (a) $t = 0$, (b) $t = 5.56$ h, (c) $t = 11.11$ h.

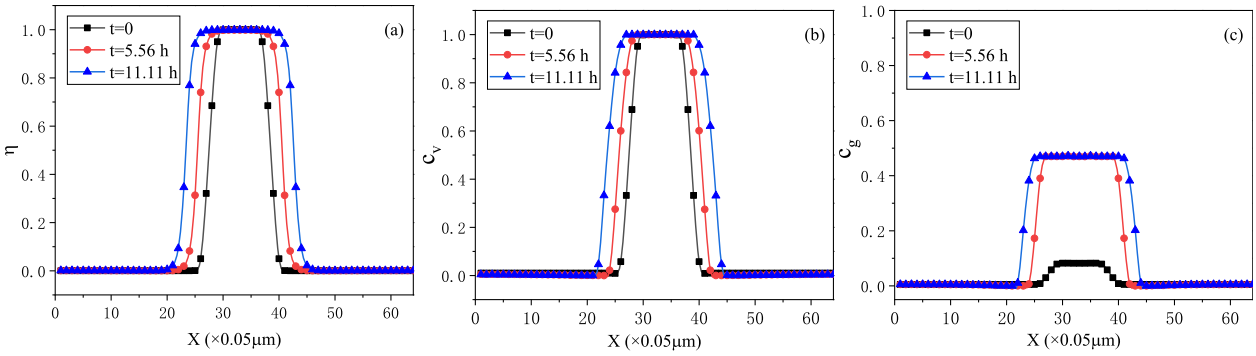

Fig. 3. Numerical distribution on the central line of the bubble (a)order parameter, (b)vacancy concentration, (c)gas atom concentration.

from the matrix, the size of bubbles increases. It should be noted that the concentration of gas atom in a bubble is affected by the flux of gas atom and the change in the bubble volume itself [26].

Based on the curve in Fig. 1, a bubble with a radius of 0.2 μm is set initially with its corresponding interior gas atom concentration of 0.082, and the simulation domain was divided into 64 × 64 grid points. In order to investigate the evolution of phase-field variables, the point defect concentration in the matrix is set as $c_v = 0.01$ and $c_g = 0.005$, which is much higher than the equilibrium concentration. The evolution of bubble morphologies is shown in Fig. 2. Due to the supersaturated vacancy and gas atom, the bubble grows to about 0.4 μm after 11.11 h. In addition, the bubble keeps circular during the whole process due to the interface energy minimization.

The distribution of phase-field variables, corresponding to Fig. 2, is shown in Fig. 3, and the initial defect concentration is set as $\eta = c_v = 1.0$ and $c_g = 0.082$ in the bubble. It is clear that the bubble radius increases with the increase of time, while the width of the diffusion interface remains the same. Moreover, the value of order parameter and vacancy concentration within the bubble is invariant while the gas atom concentration increases to its maximum due to the trend of chemical potential equalization between inside and outside of the bubble, which is similar to Xiao's work [32].

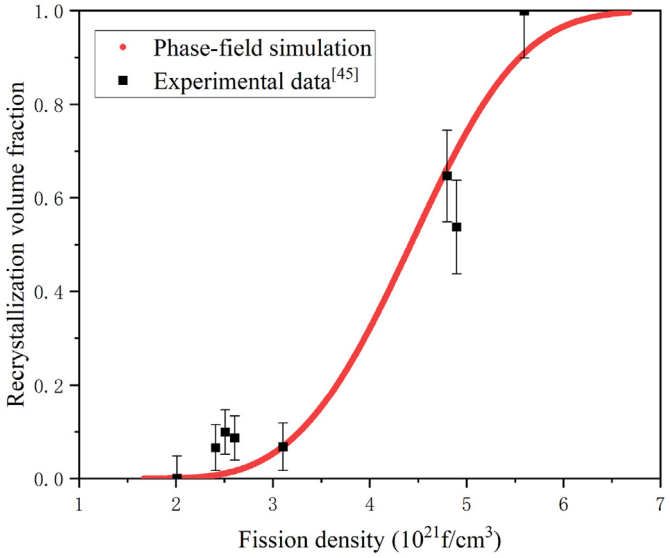

Fig. 4. Fitted recrystallization fraction as well as the corresponding experimental data as a function of fission density.

3.2. Effects of fission density on bubbles evolution

The recrystallization in U–Mo alloy plays a key role in the fission gas bubbles behavior. Based on the recrystallization kinetics characterized by the experiment in Kim's work [45], the process of recrystallization is coupled into our phase-field simulation, and a modified Avrami equation is used to describe the recrystallization kinetics of U–Mo alloy:

$$V_{rx} = 1 - \exp\left[-K(F - F_0)^n\right] \tag{27}$$

where V_{rx} is the volume fraction with recrystallized grains, K is the recrystallization reaction constant and F is the fission density with a unit of 10^{21} f/cm^3, F_0 is the minimum fission density for recrystallization to occur and n is the Avrami exponent that depends on nucleation and growth mechanism of subdivided grains.

The curve fitted from the experimental data is given in Fig. 4 with the value of parameters $K = 0.02$, $F_0 = 1.67$ and $n = 3.5$. In

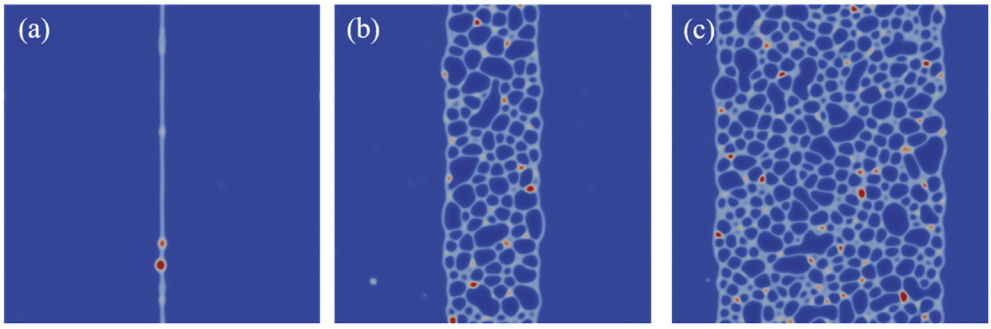

Fig. 5. The morphology evolution as a function of fission density for (a) 2.0×10^{21} f/cm^3, (b) 3.5×10^{21} f/cm^3, (c) 4.0×10^{21} f/cm^3 and (d) 4.5×10^{21} f/cm^3.

the present phase-field model, new subdivided grains are added in the system near the original GBs according to the kinetics of recrystallization.

The introduction of irradiation effects in our simulation is determined by the source items in Eqs (10) and (11). The continuously produced point defects in the irradiated materials result in the increase of vacancy and gas atom concentration in the domain which leads to bubbles formation and growth. These defects are generated randomly in space and time according to Eq. (13). To verify our model, an initial system including two recrystallized grains with an initial condition of equilibrium defect concentration was built. The simulation area is 12.8 μm × 12.8 μm and the system is initialized to contain vacancy and gas atom with $c_v = c_v^{eq}$ and $c_g = c_g^{eq}$. The evolution of the bubble and grain structures is governed by (16)–(19). In addition, 40 order parameters are used repeatedly to represent recrystallized grains that greatly speed up the calculation.

The morphology evolution under different fission densities is shown in Fig. 5 where the white region represents GB area, the red region represents bubble area and the blue region represents area within the grain. As shown in Fig. 5(a), before recrystallization, there are a few bubbles distributed in the GB. Due to the smaller free energy and faster mobility for a bubble on the GB, GB is preferential region for bubbles to form and grow [26]. An intergranular bubble will grow to lenticular and the equilibrium contact angle

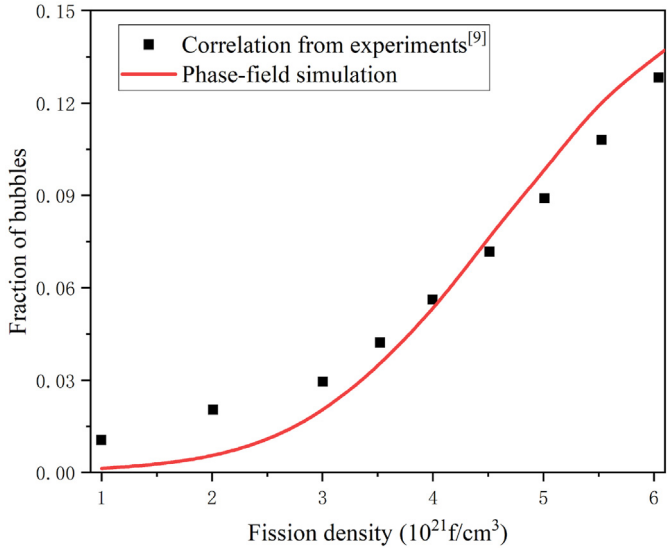

Fig. 6. Comparison between the experimental and calculated fraction of bubbles as a function of fission density.

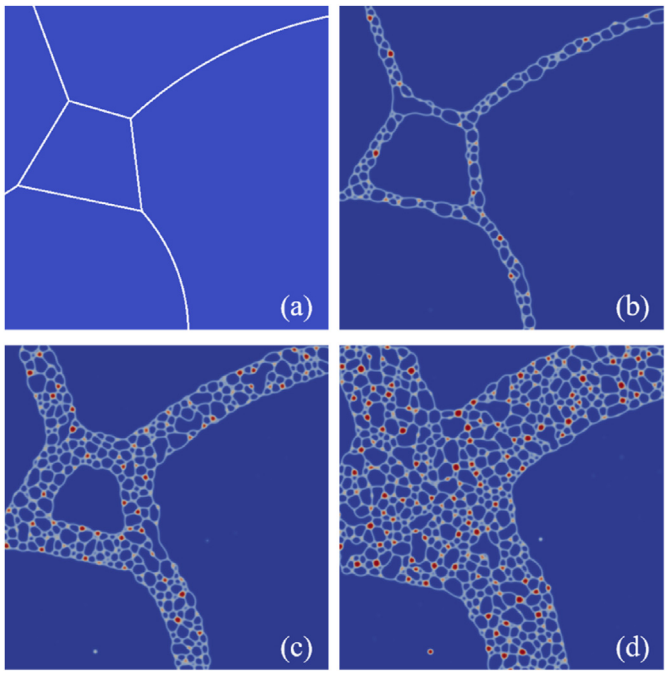

Fig. 7. The morphology evolution in polycrystalline as a function of fission density for (a) initial grains structure, (b) 3.5×10^{21} f/cm^3, (c) 4.0×10^{21} f/cm^3 and (d) 4.5×10^{21} f/cm^3.

depends on the ratio of GB energy to bubble surface energy with a form $\cos\theta = E_{GB}/2E_{surf}$ [46]. Fig. 5(b and c) show the images of bubble evolution in recrystallized U–Mo alloy. In general, the newly emerging small grains will be swallowed by the larger grains. Abundant recrystallized grains, providing GBs as sinks that absorb the point defects in the matrix and high-speed channels for gas atom migration, will store a lot of bubbles and increase intergranular bubble growth rates [47]. It is consistent with what is observed in Fig. 5(b and c) that the irradiation induced bubbles distribute among the GBs between recrystallized grains.

A set of experimental data from Kim's work [9] is used to verify our model which is shown in Fig. 6. As can be seen from the figure, our simulation is in good agreement with the experimental results overall. However, it can be seen that the fraction of bubbles is less than the experimental value at low fission density. It is deduced that the GB area is so small before recrystallization that there is a deviation that can be ignored at high fission density.

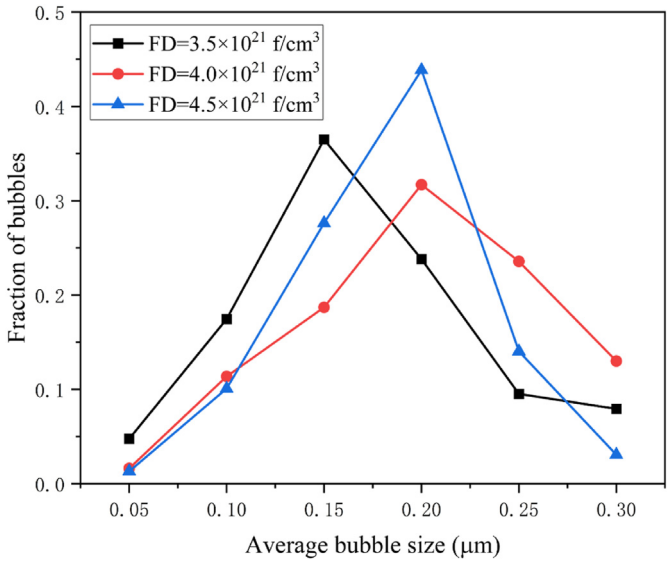

Fig. 8. Average bubble size distribution as a function of fission density.

3.3. Bubbles evolution in recrystallized polycrystalline of U–Mo alloy

In this section, the current phase-field model is employed to simulate the bubble evolution in recrystallized polycrystalline U–Mo fuel. The initial grain structure is constructed based on an experimentally observed image from Ref. [48] that contains five original grains before recrystallization. As shown in Fig. 7(a), the initial average grain size is about 10 μm with the simulation grid of 25.6 μm × 25.6 μm. The system is initialized to contain uniform vacancy and gas atom with $c_v = c_v^{eq}$ and $c_g = c_g^{eq}$, corresponding to the equilibrium conditions. The evolution of bubble and grain structures is governed by (20)–(23).

The morphology evolution of recrystallized U–Mo polycrystalline under radiation with respect to fission density are shown in Fig. 7. During irradiation, the on-going production of vacancy and gas atom leads to the supersaturated point defect concentration. Unevenly distributed defects in space cause a net flux across the bubble surfaces that allows bubbles to form and grow. Most of the bubbles are located at the GBs and triple junction regions of the recrystallized grains, and there are few bubbles in the deformed grains which is consistent with the experimental observation [48]. On the one hand, the GBs which form after recrystallization are preferential sites for bubble formation, and the newly formed GB significantly decreases the diffusion distance of gas atom from grain interior to GBs. On the other hand, there are few intragranular bubbles in the deformed grains due to the absorption of point defects by dislocation.

The size and number of bubbles significantly increase as the fission density increases. To analyze it quantitatively, the bubble size distribution as a function of fission density is plotted in Fig. 8. It can be obtained by a statistical analysis that the number of bubbles increases from 22 to 135 as the fission density increases from 3.5×10^{21} f/cm^{-3} to 4.5×10^{21} f/cm^{-3}. As shown by the black and red lines in Fig. 8, the peak of the bubble size distribution shifts to the larger size side when the fission density increases. The reason for this shift is that, bubbles can grow faster by absorbing vacancies and gas atoms with higher defect supersaturation. Besides, with the increase of fission rate, both the formation rate and number density of bubbles increase. Interestingly, when the fission density increases from 4.0×10^{21} f/cm^{-3} to 4.5×10^{21} f/cm^{-3}, the number and density of bubbles have increased significantly but the peak of bubble size seems to be unchanged. Hence, it is deduced that the increment of recrystallization fraction is larger than that of point defect. The recrystallized structure provides a large GB area as a preferential nucleation region. However, the nucleation of bubbles exhausts the surrounding point defects and this is why the bubble size did not increase.

4. Conclusions

A two-dimensional phase-field model was developed to simulate the bubble evolution during radiation in recrystallized U–Mo alloy. The main conclusions can be drawn as follows:

(1). The growth of gas bubbles depends on their absorption of the supersaturated vacancies and gas atoms in the matrix. Due to the hydrostatic pressure balance, different sizes of bubbles have different corresponding equilibrium gas atom concentrations.
(2). During irradiation, both the average size and number density of bubbles increase with the increase of fission density. However, the fraction of bubbles is obviously less than the experimental value at low fission density, since the GB area is so small before recrystallization that there is a deviation which can be ignored at high fission density.
(3). In the recrystallized microstructure, bubbles with small average size and high number density were formed, since recrystallized grains with a large area fraction of GB and extremely small value of grain size significantly increase the formation probability of gas bubbles and reduces the diffusion time of gas atom from grain interior to GBs.

Declaration of competing interest

The authors declare that they have no known competing financial interests or personal relationships that could have appeared to influence the work reported in this paper.

Acknowledgements

Financial support provided by the NSAF Joint Fund (No. U1830124), National Natural Science Foundation of China (No. 11675154, 11675126, 11705137) and China Postdoctoral Science Foundation (No. 2019M663738) is acknowledged.

References

[1] J.L. Snelgrove, G.L. Hofman, M.K. Meyer, Development of very-high-density low-enriched-uranium fuels, Nucl. Eng. Des. 178 (1997) 119–126, https://doi.org/10.1016/s0029-5493(97)00217-3.
[2] D.D. Keiser, S.L. Hayes, M.L. Meyer, High-density, low-enriched uranium fuel for nuclear research reactors, JOM (J. Occup. Med.) 55 (2003) 55–58, https://doi.org/10.1007/s11837-003-0031-0.
[3] S. Van den Berghe, P. Lemoine, Review of 15 years of high-density low-enriched UMo dispersion fuel development for research reactors in Europe, Nucl. Eng. Technol. 46 (2014) 125–146, https://doi.org/10.5516/NET.07.2014.703.
[4] M.K. Meyer, G.L. Hofman, S.L. Hayes, Low-temperature irradiation behavior of uranium–molybdenum alloy dispersion fuel, J. Nucl. Mater. 304 (2002) 221–236, https://doi.org/10.1016/S0022-3115(02)00850-4.
[5] D.R. Olander, Fundamental Aspects of Nuclear Reactor Fuel Elements: Solutions to Problems, California Univ, Berkeley (USA), 1976. Dept. of Nuclear Engineering.
[6] G.L. Hofman, G.L. Copeland, J.E. Sanecki, Microscopic investigation into the irradiation behavior of U_3O_8-Al dispersion fuel, Nucl. Technol. 72 (1986) 338–344, https://doi.org/10.13182/NT86-A33772.
[7] R.M. Berman, Fission fragment distribution in irradiated UO_2, Nucl. Sci. Eng. 16 (1963) 315–328, https://doi.org/10.13182/NSE63-A26534.
[8] J. Gan, D.D. Keiser, B.D. Miller, TEM characterization of U–7Mo/Al–2Si

dispersion fuel irradiated to intermediate and high fission densities, J. Nucl. Mater. 424 (2012) 43–50, https://doi.org/10.1016/j.jnucmat.2012.02.001.
[9] Y.S. Kim, G.L. Hofman, Fission product induced swelling of U–Mo alloy fuel, J. Nucl. Mater. 419 (2011) 291–301, https://doi.org/10.1016/j.jnucmat.2011.08.018.
[10] J. Spino, D. Baron, M. Coquerelle, High burn-up rim structure: evidences that xenon-depletion, pore formation and grain subdivision start at different local burn-ups, J. Nucl. Mater. 256 (1998) 189–196, https://doi.org/10.1016/S0022-3115(98)00060-9.
[11] S. Kashibe, K. Une, K. Nogita, Formation and growth of intragranular fission gas bubbles in UO_2 fuels with burnup of 6–83 GWd/t, J. Nucl. Mater. 206 (1993) 22–34, https://doi.org/10.1016/0022-3115(93)90229-R.
[12] H. Matzke, On the rim effect in high burnup UO_2 LWR fuels, JNuM 189 (1992) 141–148, https://doi.org/10.1016/0022-3115(92)90428-N.
[13] K. Nogita, K. Une, Radiation-induced microstructural change in high burnup UO_2 fuel pellets, Nucl. Instrum. Methods Phys. Res., Sect. B 91 (1994) 301–306, https://doi.org/10.1016/0168-583X(94)96235-9.
[14] V.V. Rondinella, T. Wiss, The high burn-up structure in nuclear fuel, Mater. Today 13 (2010) 24–32, https://doi.org/10.1016/S1369-7021(10)70221-2.
[15] J. Noirot, L. Desgranges, J. Lamontagne, Detailed characterizations of high burn-up structures in oxide fuels, J. Nucl. Mater. 372 (2008) 318–339, https://doi.org/10.1016/j.jnucmat.2007.04.037.
[16] J. Spino, K. Vennix, M. Coquerelle, Detailed characterisation of the rim microstructure in PWR fuels in the burn-up range 40–67 GWd/tM, J. Nucl. Mater. 231 (1996) 179–190, https://doi.org/10.1016/0022-3115(96)00374-1.
[17] S.Y. Hu, W. Setyawan, V.V. Joshi, Atomistic simulations of thermodynamic properties of Xe gas bubbles in U10Mo fuels, J. Nucl. Mater. 490 (2017) 49–58, https://doi.org/10.1016/j.jnucmat.2017.04.016.
[18] H.X. Xiao, C.S. Long, X.F. Tian, Atomistic simulations of the small xenon bubble behavior in U-Mo alloy, Mater. Des. 74 (2015) 55–60, https://doi.org/10.1016/j.matdes.2015.02.005.
[19] J. Rest, A model for the influence of microstructure, precipitate pinning and fission gas behavior on irradiation-induced recrystallization of nuclear fuels, J. Nucl. Mater. 326 (2004) 175–184, https://doi.org/10.1016/j.jnucmat.2004.01.009.
[20] J. Rest, Model for the effect of the progression of irradiation-induced recrystallization from initiation to completion on swelling of UO_2 and U–10Mo nuclear fuels, J. Nucl. Mater. 324 (2005) 226–232, https://doi.org/10.1016/j.jnucmat.2005.06.012.
[21] M.R. Tonks, D. Gaston, C. Permann, A coupling methodology for mesoscale-informed nuclear fuel performance codes, Nucl. Eng. Des. 240 (2010) 2877–2883, https://doi.org/10.1016/j.nucengdes.2010.06.005.
[22] A. Cheniour, M.R. Tonks, B. Gong, Development of a grain growth model for U3Si2 using experimental data, phase field simulation and molecular dynamics, J. Nucl. Mater. (2020) 152069, https://doi.org/10.1016/j.jnucmat.2020.152069.
[23] Z.G. Mei, L. Liang, Y.S. Kim, Grain growth in U–7Mo alloy: a combined first-principles and phase field study, J. Nucl. Mater. 473 (2016) 300–308, https://doi.org/10.1016/j.jnucmat.2016.01.027.
[24] Y.B. Jiang, W.B. Liu, W.J. Li, Phase-field simulation of the interaction between intergranular voids and grain boundaries during radiation in UO_2, Comput. Mater. Sci. (2020) 110176, https://doi.org/10.1016/j.commatsci.2020.110176.
[25] L. Liang, Z.G. Mei, Y.S. Kim, Three-dimensional phase-field simulations of intragranular gas bubble evolution in irradiated U-Mo fuel, Comput. Mater. Sci. 145 (2018) 86–95, https://doi.org/10.1016/j.commatsci.2017.12.061.
[26] P.C. Millett, A. El-Azab, D. Wolf, Phase-field simulation of irradiated metals: Part II: gas bubble kinetics, Comput. Mater. Sci. 50 (2011) 960–970, https://doi.org/10.1016/j.commatsci.2010.10.032.
[27] M.G. Abdoelatef, F. Badry, D. Schwen, Mesoscale modeling of high burn-up structure formation and evolution in UO_2, JOM (J. Occup. Med.) 71 (2019) 4817–4828, https://doi.org/10.1007/s11837-019-03830-z.
[28] L. Liang, Y.S. Kim, Z.G. Mei, Fission gas bubbles and recrystallization-induced degradation of the effective thermal conductivity in U-7Mo fuels, J. Nucl. Mater. 511 (2018) 438–445, https://doi.org/10.1016/j.jnucmat.2018.09.054.
[29] L. Liang, Z.G. Mei, A.M. Yacout, Fission-induced recrystallization effect on intergranular bubble-driven swelling in U-Mo fuel, Comput. Mater. Sci. 138 (2017) 16–26, https://doi.org/10.1016/j.commatsci.2017.06.013.
[30] S. Hu, V. Joshi, C.A. Lavender, A rate-theory–phase-field model of irradiation-induced recrystallization in UMo nuclear fuels, JOM (J. Occup. Med.) 69 (2017) 2554–2562, https://doi.org/10.1007/s11837-017-2611-4.
[31] L.Q. Chen, Y. Wei, Computer simulation of the domain dynamics of a quenched system with a large number of nonconserved order parameters: the grain-growth kinetics, Phys. Rev. B 50 (1994) 15752, https://doi.org/10.1103/PhysRevB.50.15752.
[32] Z. Xiao, Y. Wang, S. Hu, A quantitative phase-field model of gas bubble evolution in UO_2, Comput. Mater. Sci. 184 (2020) 109867, https://doi.org/10.1016/j.commatsci.2020.109867.
[33] J.W. Cahn, J.E. Hilliard, Free energy of a nonuniform system. I. Interfacial free energy, J. Chem. Phys. 28 (1958) 258–267, https://doi.org/10.1063/1.1744102.
[34] Y. Wang, Z. Xiao, S. Hu, A phase field study of the thermal migration of gas bubbles in UO_2 nuclear fuel under temperature gradient, Comput. Mater. Sci. 183 (2020) 109817, https://doi.org/10.1016/j.commatsci.2020.109817.
[35] I. Steinbach, Phase-field model for microstructure evolution at the mesoscopic scale, Annu. Rev. Mater. Res. 43 (2013) 89–107, https://doi.org/10.1146/annurev-matsci-071312-121703.
[36] P.C. Millett, A. El-Azab, S. Rokkam, Phase-field simulation of irradiated metals: Part I: void kinetics, Comput. Mater. Sci. 50 (2011) 949–959, https://doi.org/10.1016/j.commatsci.2010.10.034.
[37] J. Rest, G.L. Hofman, Effect of recrystallization in high-burnup UO{sub 2} on gas release during RIA-type transients, 1994, https://doi.org/10.2172/432943. ANL/ET/PP–84776.
[38] N. Moelans, A quantitative and thermodynamically consistent phase-field interpolation function for multi-phase systems, Acta Mater. 59 (2011) 1077–1086, https://doi.org/10.1016/j.actamat.2010.10.038.
[39] J. Rest, An analytical study of gas-bubble nucleation mechanisms in uranium-alloy nuclear fuel at high temperature, J. Nucl. Mater. 402 (2010) 179–185, https://doi.org/10.1016/j.jnucmat.2010.05.022.
[40] D.R. Olander, Fundamental Aspects of Nuclear Reactor Fuel Elements, United State, 1976, https://doi.org/10.2172/7343826. TID-26711-P1.
[41] Z.G. Mei, L. Liang, A.M. Yacout, First-principles study of the surface properties of U-Mo system, Comput. Mater. Sci. 142 (2018) 355–360, https://doi.org/10.1016/j.commatsci.2017.10.033.
[42] R.C. Reid, J.M. Prausnitz, B.E. Poling, The Properties of Gases and Liquids, 1987. United States.
[43] S. Hu, A.M. Casella, C.A. Lavender, Assessment of effective thermal conductivity in U–Mo metallic fuels with distributed gas bubbles, J. Nucl. Mater. 462 (2015) 64–76, https://doi.org/10.1016/j.jnucmat.2015.03.039.
[44] N. Moelans, B. Blanpain, P. Wollants, Quantitative analysis of grain boundary properties in a generalized phase field model for grain growth in anisotropic systems, Phys. Rev. B 78 (2008), 024113, https://doi.org/10.1103/PhysRevB.78.024113.
[45] Y.S. Kim, G.L. Hofman, J.S. Cheon, Recrystallization and fission-gas-bubble swelling of U-Mo fuel, J. Nucl. Mater. 436 (2013) 14–22, https://doi.org/10.1016/j.jnucmat.2013.01.291.
[46] P.C. Millett, M.R. Tonks, S.B. Biner, Phase-field simulation of intergranular bubble growth and percolation in biocrystals, J. Nucl. Mater. 425 (2012) 130–135, https://doi.org/10.1016/j.jnucmat.2011.07.034.
[47] J. Rest, The effect of irradiation-induced gas-atom re-solution on grain-boundary bubble growth, J. Nucl. Mater. 321 (2003) 305–312, https://doi.org/10.1016/S0022-3115(03)00303-9.
[48] Y.S. Kim, J.M. Park, K.H. Lee, In-pile test results of U-silicide or U-nitride coated U-7Mo particle dispersion fuel in Al, J. Nucl. Mater. 454 (2014) 238–246, https://doi.org/10.1016/j.jnucmat.2014.08.005.